LETTERS
https://doi.org/10.1038/s41558-020-0697-0

nature climate change

Check for updates

Sandy coastlines under threat of erosion

Michalis I. Vousdoukas[1]✉, Roshanka Ranasinghe[2,3,4], Lorenzo Mentaschi[1], Theocharis A. Plomaritis[5,6], Panagiotis Athanasiou[3,4], Arjen Luijendijk[4,7] and Luc Feyen[1]

Sandy beaches occupy more than one-third of the global coastline[1] and have high socioeconomic value related to recreation, tourism and ecosystem services[2]. Beaches are the interface between land and ocean, providing coastal protection from marine storms and cyclones[3]. However the presence of sandy beaches cannot be taken for granted, as they are under constant change, driven by meteorological[4,5], geological[6] and anthropogenic factors[1,7]. A substantial proportion of the world's sandy coastline is already eroding[1,7], a situation that could be exacerbated by climate change[8,9]. Here, we show that ambient trends in shoreline dynamics, combined with coastal recession driven by sea level rise, could result in the near extinction of almost half of the world's sandy beaches by the end of the century. Moderate GHG emission mitigation could prevent 40% of shoreline retreat. Projected shoreline dynamics are dominated by sea level rise for the majority of sandy beaches, but in certain regions the erosive trend is counteracted by accretive ambient shoreline changes; for example, in the Amazon, East and Southeast Asia and the north tropical Pacific. A substantial proportion of the threatened sandy shorelines are in densely populated areas, underlining the need for the design and implementation of effective adaptive measures.

The coastal zone is among the most developed areas worldwide, containing an abundance of developments, critical infrastructure[10] and ecosystems[2,3]. As a result, population density tends to be higher near the coast[11]. Most projections indicate that current trends of coastward migration, urbanization and population growth will continue[12,13]. Of the different beach typologies found worldwide sandy beaches are the most heavily used[14] and are among the most geomorphologically complex, with the shoreline (the mean water line along the coast) changing constantly under forcing–response interactions between natural and anthropogenic factors[7].

The global mean sea level has been increasing at an accelerated rate during the past 25 years[15] and will continue to do so with climate change[16,17]. While shoreline change can be the combined result of a wide range of potentially erosive or accretive factors[8], there is a clear cause and effect relationship between increasing sea levels and shoreline retreat[18], pointing to increased coastal erosion issues[9,19]. Climate change will also affect waves and storm surges[20,21], which are important drivers of coastal morphology[4,5,22]. Therefore, considering the dynamics of extreme weather patterns is also important in assessing potential climate change impacts beyond that of sea-level rise (SLR) alone.

Here, we present a comprehensive global analysis of sandy shoreline dynamics during the twenty-first century. Our probabilistic projections explicitly take into account estimates of future SLR, spatial variations of coastal morphology, ambient shoreline change trends and future changes in meteorological drivers (for example, storm surge and waves). We first evaluate long-term shoreline change $dx_{\mathrm{shore\_LT}}$, which is the result of two components: the ambient shoreline change (AC) driven by geological, anthropogenic and other physical factors[7] and the shoreline retreat due to SLR (R) (Supplementary Fig. 1). We obtained AC by extrapolating observed historical trends[1,7] within a probabilistic framework (see Methods). We computed R by using a modified Bruun rule[18] together with a new global dataset of active beach slopes[23]. In addition to the long-term shoreline dynamics we also project how maximum erosion from coastal storms may change with climate change. Shoreline change projections are discussed for the years 2050 and 2100 under representative concentration pathways (RCP) 4.5 and 8.5, relative to the baseline year 2010.

Our analysis shows an overall erosive trend of sandy beaches that increases in time and with the intensity of GHG emissions (Fig. 1). Assuming that there are no physical limits in potential coastal retreat, by mid-century we project a probable (5th–95th percentile) global average long-term shoreline change $dx_{\mathrm{shore,LT}}$ ranging from −78.1 to −1.1 m and −98.1 to 0.3 m, under RCP 4.5 and RCP 8.5, respectively (negative values express erosion; Supplementary Table 1). By the end of the century the erosive trend becomes even more dominant and we project a probable range from −164.2 to −14.8 m and −240 to −35.3 m under RCP 4.5 and RCP 8.5, respectively (Fig. 2 and Supplementary Table 1). Moderate GHG emission mitigation could thus prevent 17% of the projected shoreline retreat by 2050 and 40% by the end of the century (Supplementary Table 1). This corresponds to a global average of around 42 m of preserved sandy beach width by the end of the century.

The global erosive trend masks high spatial variability, with erosive and accretive tendencies interchanging across regions and along nearby coastal segments (Fig. 1). Local trends can exceed several metres per year, while 11 IPCC subregions show median retreats exceeding 100 m under both RCPs by the end of the century (Supplementary Table 1; see Fig. 2 for a definition of the regions): central and eastern North America, Central America and Mexico, southeastern South America, central Europe, East and West Africa, South Asia, North Australia as well as the Pacific and Caribbean. Small Island Developing States (SIDS). By 2100, $dx_{\mathrm{shore,LT}}$ exceeds 150 m under RCP 8.5 in most of the above regions, while under the same scenario median retreats larger than 200 m are projected for central North America, South Asia, North Australia and the Caribbean SIDS.

SLR-driven retreat R is responsible for 73% and 77% of the global median shoreline change in 2050 under RCP 4.5 and RCP 8.5,

[1]European Commission, Joint Research Centre (JRC), Ispra, Italy. [2]Department of Water Science and Engineering, IHE Delft Institute for Water Education, Delft, the Netherlands. [3]Water Engineering and Management, Faculty of Engineering Technology, University of Twente, Enschede, the Netherlands. [4]Harbour, Coastal and Offshore Engineering, Deltares, Delft, the Netherlands. [5]Department of Applied Physics, CASEM, University of Cadiz, Cadiz, Spain. [6]CIMA, University of Algarve, Campus de Gambelas, Faro, Portugal. [7]Department of Hydraulic Engineering, Faculty of Civil Engineering and Geosciences, Delft University of Technology, Delft, the Netherlands. ✉e-mail: Michail.VOUSDOUKAS@ec.europa.eu

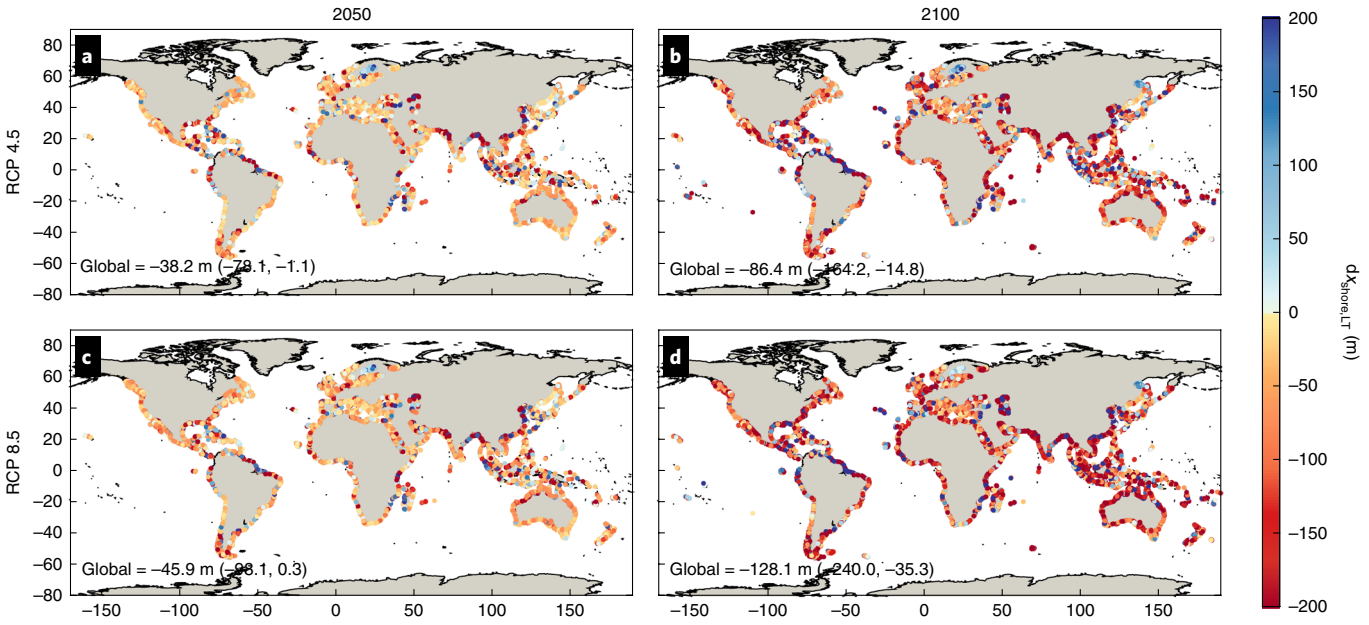

Fig. 1 | Projected long-term shoreline changes. a–d, Projected shoreline changes by the years 2050 (**a**,**c**) and 2100 (**b**,**d**) under RCP 4.5 (**a**,**b**) and RCP 8.5 (**c**,**d**). Values represent the median change and positive/negative values, respectively, express accretion/erosion in metres, relative to 2010. The global average median change is shown in the inset text for each case, along with the 5th–95th percentile range.

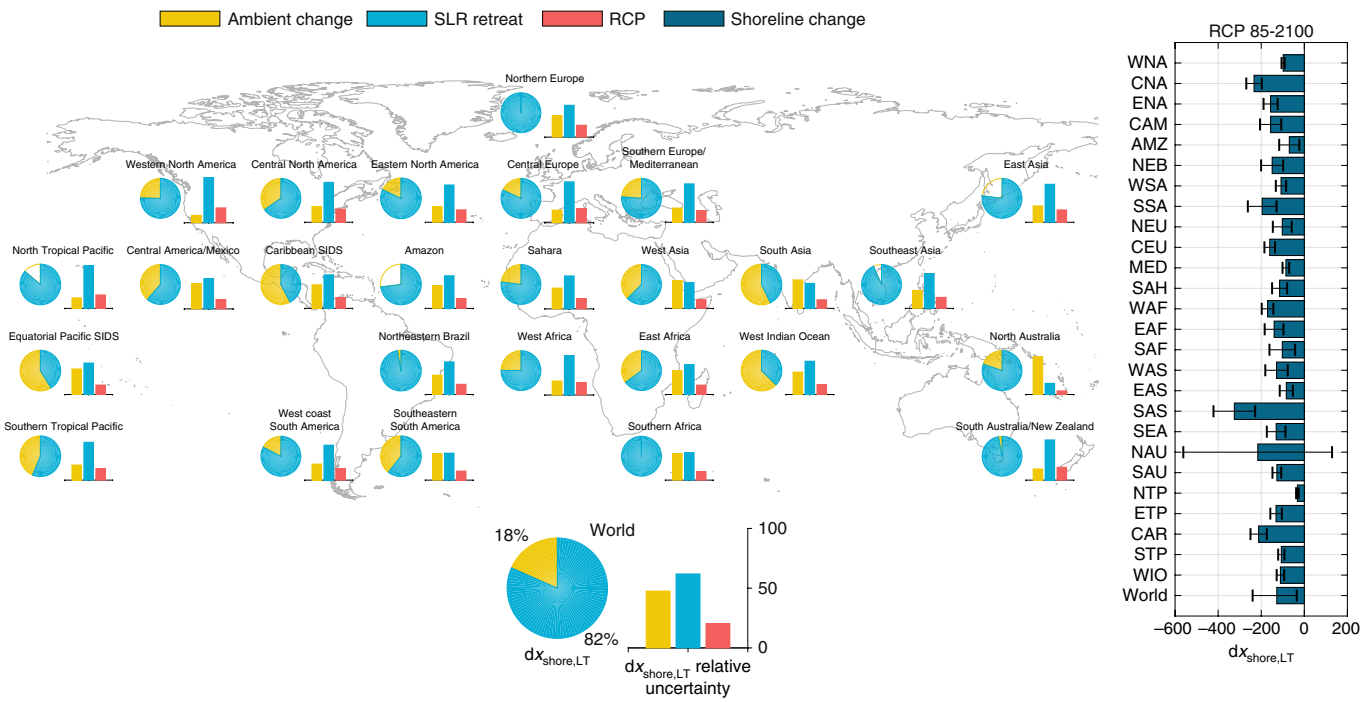

Fig. 2 | Projected median long-term shoreline change under RCP 8.5 by the year 2100 ($dx_{shore,LT}$), for the 26 IPCC SREX subregions and the worldwide average. For the horizontal bar plot on the right; positive/negative values express accretion/erosion in metres; black error bars indicate the 5th–95th quantile range. Shoreline change is considered to be the result of SLR retreat (*R*) and ambient shoreline change trends (AC). Pie plots show the relative contributions of *R* and AC to the projected median $dx_{shore,LT}$, with transparent slices expressing accretive trends. Vertical bar plots show the ratio between the uncertainty of *R* and AC (5th–95th quantile range), to the total uncertainty in projected median $dx_{shore,LT}$. WNA, Western North America; CNA, Central North America; ENA, Eastern North America; CAM, Central America/Mexico; AMZ, Amazon; NEB, Northeastern Brazil; WSA, Western South America; SSA, Southeastern South America; NEU, Northern Europe; CEU, Central Europe; MED, Mediterranean; SAH, Sahara; WAF, West Africa; EAF, East Africa; SAF, Southern Africa; WAS, West Asia; EAS, East Asia; SAS, South Asia; SEA, Southeast Asia; NAU, North Australia; SAU, South Australia; NTP, North Tropical Pacific; ETP, Equatorial Pacific SIDS; CAR, Caribbean SIDS; STP, Southern Tropical Pacific; WIO, West Indian Ocean.

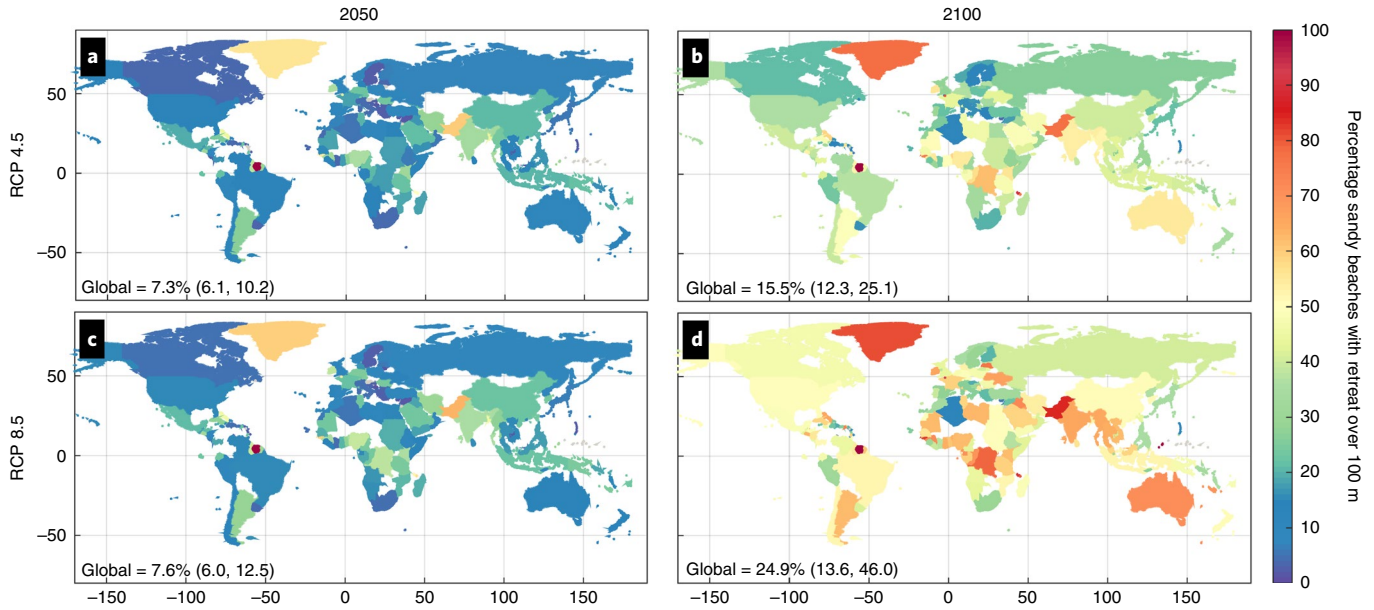

Fig. 3 | Per country percentage of sandy beach coastline projected to experience critical erosion. a–d, Percentages per country of sandy coastline length projected to retreat by >100 m by 2050 (**a**,**c**) and 2100 (**b**,**d**), under RCP 4.5 (**a**,**b**) and RCP 8.5 (**c**,**d**). Values are based on the median long-term shoreline change relative to 2010. The global average percentage of sandy beaches projected to retreat by >100 m is shown in the inset text for each case; values express the median along with the 5th–95th percentile range.

respectively (Extended Data Figs. 5 and 6); and for 73% and 85% by the end of the century (Fig. 2 and Extended Data Fig. 7). Ambient shoreline changes dominate only in certain regions, in particular in the west Indian Ocean, Caribbean and Pacific SIDS, and South and West Asia. The contributions of the SLR retreat and ambient change to the overall uncertainty under RCP 4.5 and by mid-century are relatively balanced (Extended Data Fig. 5), while AC contributes to 41% more uncertainty globally by the end of the century (Extended Data Fig. 7). Under RCP 8.5 uncertainty related to SLR retreat dominates that of AC by 44% and 30% by the years 2050 and 2100, respectively (Extended Data Figs. 7 and 2). Regionally, ambient change uncertainty is higher in North Australia and South Asia.

The above estimates do not include the episodic, storm-driven shoreline retreat S, presently projected using the convolution erosion model of Kriebel and Dean[24] (see Methods). Here, we discuss the 100-yr event S which for the year 2050 is equivalent to about 23% of the global average projected long-term shoreline change $dx_{shore,LT}$ (Supplementary Tables 1–4). By the end of the twenty-first century, the relative importance of the 100-yr S compared to $dx_{shore,LT}$ decreases to 9% and 7% under RCP 4.5 and 8.5, respectively, as long-term changes gather pace. Storm erosion is typically followed by beach recovery[25] but some events may leave a footprint that takes decades to recover, if at all[4,26], while the additional shoreline retreat renders the backshore more vulnerable to episodic coastal flooding and its consequences. Despite previous studies projecting changes in wave intensity and direction worldwide[21,27,28], our projections show that overall climate change will not have a strong effect on episodic storm-driven erosion. As a result, ambient and SLR-driven change appear to shadow the effect of changes in storm-driven erosion, even though at certain locations ΔS values can reach ±20 m by the end of the century; for example, increase in 100-yr erosion potential along the southeastern coast of the United Kingdom, west coast of Germany, North Queensland (Australia) and Acapulco (Mexico) (Extended Data Fig. 4).

The projected shoreline changes will substantially impact the shape of the world's coastline. Many coastal systems have already lost their natural capacity to accommodate or recover from erosion, as the backshore is heavily occupied by human settlements[29], while dams and human development have depleted terrestrial sediment supply which would naturally replenish the shore with new material[30,31]. Most of the remaining regions with an extensive presence of a natural coastline, are found in Africa and Asia, which are also the regions projected to experience the highest coastal population and urbanization growth in the decades to come[12,13]. There is yet no global dataset on sandy beach width allowing us to accurately estimate the potential loss of sandy beaches around the world. Therefore, to quantify the potential impact of our projections, we consider beaches that are projected to experience a shoreline retreat >100 m as seriously threatened by coastal erosion. The chosen 100-m threshold is conservative, since most sandy beaches have widths below 50 m, especially near human settlements, small islands and micro-tidal areas (for example, Caribbean and Mediterranean).

We find that 13.6–15.2% (36,097–40,511 km) of the world's sandy beaches could face severe erosion by 2050, a number rising to 35.7–49.5% (95,061–131,745 km) by the end of the century (Extended Data Fig. 8). A total 31% of the world's sandy beaches are in low-elevation coastal zones with population density exceeding 500 people per km^2, and our projections show that about one-third of these low-elevation coastal zones will be seriously threatened by erosion by 2050. This estimate reaches 52% and 63% by the end of the century, under RCP 4.5 and RCP 8.5, respectively.

Several countries could face extensive sandy beach erosion issues by the end of the twenty-first century (affecting >60% of their sandy coastline under both RCPs; Fig. 3) including the Democratic Republic of the Congo, Gambia, Jersey, Suriname, Comoros, Guinea-Bissau, Pakistan and Mayotte (France). Apart from the consequent higher vulnerability to coastal hazards, several of these countries are likely to experience substantial socioeconomic implications as their economies are fragile and tourism-dependent, with sandy coastlines constituting their major tourist attraction. When the total length of sandy beaches projected to be lost by 2100 is considered (as opposed to the percentage), Australia emerges as the potentially most affected country, with at least 11,426 km of sandy beach coastline threatened by erosion (14,849 km under RCP 8.5;

Extended Data Fig. 9), equivalent to ~50% of the country's total sandy coastline. By the same impact metric, Canada ranks second (6,426 and 14,425 km under RCP 4.5 and RCP 8.5, respectively), followed by Chile (5,042 and 6,659 km), Mexico (4,507 and 5,488 km), China (4,300 and 5,440 km), USA (3,945 and 5,530 km), Russia (3,056 and 4,762 km) and Argentina (2,948 and 3,739 km).

Past experience has shown that effective site-specific coastal planning can mitigate beach erosion, eventually resulting in a stable coastline; with the most prominent example being the Dutch coast[32]. A positive message from the present analysis is that while SLR will drive shoreline retreat almost everywhere, many locations show ambient erosive trends related to human interventions[7], which in theory could be avoided by more sustainable coastal zone and catchment management practices. At the same time, the range of projected SLR implies unprecedented pressure to our coasts, which requires the development and implementation of informed and effective adaptive measures.

Online content

Any methods, additional references, Nature Research reporting summaries, source data, extended data, supplementary information, acknowledgements, peer review information; details of author contributions and competing interests; and statements of data and code availability are available at https://doi.org/10.1038/s41558-020-0697-0.

Received: 24 June 2019; Accepted: 8 January 2020;
Published online: 2 March 2020

References

1. Luijendijk, A. et al. The state of the world's beaches. *Sci. Rep.* **8**, 6641 (2018).
2. Barbier, E. B. et al. The value of estuarine and coastal ecosystem services. *Ecol. Monogr.* **81**, 169–193 (2011).
3. Temmerman, S. et al. Ecosystem-based coastal defence in the face of global change. *Nature* **504**, 79–83 (2013).
4. Masselink, G. et al. Extreme wave activity during 2013/2014 winter and morphological impacts along the Atlantic coast of Europe. *Geophys. Res. Lett.* **43**, 2135–2143 (2016).
5. Barnard, P. L. et al. Coastal vulnerability across the Pacific dominated by El Niño/Southern oscillation. *Nat. Geosci.* **8**, 801–807 (2015).
6. Cooper, J. A. G., Green, A. N. & Loureiro, C. Geological constraints on mesoscale coastal barrier behaviour. *Glob. Planet. Change* **168**, 15–34 (2018).
7. Mentaschi, L., Vousdoukas, M. I., Pekel, J.-F., Voukouvalas, E. & Feyen, L. Global long-term observations of coastal erosion and accretion. *Sci. Rep.* **8**, 12876 (2018).
8. Ranasinghe, R. Assessing climate change impacts on open sandy coasts: a review. *Earth Sci. Rev.* **160**, 320–332 (2016).
9. Hinkel, J. et al. A global analysis of erosion of sandy beaches and sea-level rise: an application of DIVA. *Glob. Planet. Change* **111**, 150–158 (2013).
10. Koks, E. E. et al. A global multi-hazard risk analysis of road and railway infrastructure assets. *Nat. Commun.* **10**, 2677 (2019).
11. McGranahan, G., Balk, D. & Anderson, B. The rising tide: assessing the risks of climate change and human settlements in low elevation coastal zones. *Environ. Urban.* **19**, 17–37 (2007).
12. Neumann, B., Vafeidis, A. T., Zimmermann, J. & Nicholls, R. J. Future coastal population growth and exposure to sea-level rise and coastal flooding—a global assessment. *PLoS ONE* **10**, e0118571 (2015).
13. Jones, B. & O'Neill, B. C. Spatially explicit global population scenarios consistent with the Shared Socioeconomic Pathways. *Environ. Res. Lett.* **11**, 8 (2016).
14. Davenport, J. & Davenport, J. L. The impact of tourism and personal leisure transport on coastal environments: a review. *Estuar. Coast. Shelf Sci.* **67**, 280–292 (2006).
15. Nerem, R. S. et al. Climate-change-driven accelerated sea-level rise detected in the altimeter era. *Proc. Natl Acad. Sci. USA* **115**, 2022–2025 (2018).
16. Bamber, J. L., Oppenheimer, M., Kopp, R. E., Aspinall, W. P. & Cooke, R. M. Ice sheet contributions to future sea-level rise from structured expert judgment. *Proc. Natl Acad. Sci. USA* **116**, 11195–11200 (2019).
17. Jevrejeva, S., Jackson, L. P., Riva, R. E. M., Grinsted, A. & Moore, J. C. Coastal sea level rise with warming above 2 °C. *Proc. Natl Acad. Sci. USA* **113**, 13342–13347 (2016).
18. Bruun, P. Sea level rise as a cause of shore erosion. *J. Waterw. Harb. Div.* **88**, 117–130 (1962).
19. Anthony, E. J. et al. Linking rapid erosion of the Mekong river delta to human activities. *Sci. Rep.* **5**, 14745 (2015).
20. Vousdoukas, M. I. et al. Global probabilistic projections of extreme sea levels show intensification of coastal flood hazard. *Nat. Commun.* **9**, 2360 (2018).
21. Hemer, M. A., Fan, Y., Mori, N., Semedo, A. & Wang, X. L. Projected changes in wave climate from a multi-model ensemble. *Nat. Clim. Change* **3**, 471–476 (2013).
22. Slott, J. M., Murray, A. B., Ashton, A. D. & Crowley, T. J. Coastline responses to changing storm patterns. *Geophys. Res. Lett.* **33**, https://doi.org/10.1029/2006GL027445 (2006).
23. Athanasiou, P. et al. Global distribution of nearshore slopes with implications for coastal retreat. *Earth Syst. Sci. Data* **11**, 1515–1529 (2019).
24. Kriebel, D. L. & Dean, R. G. Convolution method for time dependent beach profile response. *J. Waterw. Port Coast. Ocean Eng.* **119**, 204–226 (1993).
25. Vousdoukas, M. I. Erosion/accretion patterns and multiple beach cusp systems on a meso-tidal, steeply-sloping beach. *Geomorphology* **141**, 34–46 (2012).
26. Anderson, T. R., Frazer, L. N. & Fletcher, C. H. Transient and persistent shoreline change from a storm. *Geophys. Res. Lett.* **37**, L08401 (2010).
27. Erikson, L. H., Hegermiller, C. A., Barnard, P. L., Ruggiero, P. & van Ormondt, M. Projected wave conditions in the Eastern North Pacific under the influence of two CMIP5 climate scenarios. *Ocean Model.* **96**, 171–185 (2015).
28. Mentaschi, L., Vousdoukas, M. I., Voukouvalas, E., Dosio, A. & Feyen, L. Global changes of extreme coastal wave energy fluxes triggered by intensified teleconnection patterns. *Geophys. Res. Lett.* **44**, 2416–2426 (2017).
29. Small, C. & Nicholls, R. J. A global analysis of human settlement in coastal zones. *J. Coast. Res.* **19**, 584–599 (2003).
30. Milliman, J. D. Blessed dams or damned dams? *Nature* **386**, 325–327 (1997).
31. Ranasinghe, R., Wu, C. S., Conallin, J., Duong, T. M. & Anthony, E. J. Disentangling the relative impacts of climate change and human activities on fluvial sediment supply to the coast by the world's large rivers: Pearl River Basin, China. *Sci. Rep.* **9**, 9236 (2019).
32. Brière, C., Janssen, S. K. H., Oost, A. P., Taal, M. & Tonnon, P. K. Usability of the climate-resilient nature-based sand motor pilot, the Netherlands. *J. Coast. Conserv.* **22**, 491–502 (2018).

Methods

General concepts. In this study, we project shoreline dynamics throughout this century along the world's sandy coastlines under two RCPs: RCP 4.5 and RCP 8.5. RCP 4.5 may be viewed as a moderate-emission mitigation-policy scenario and RCP 8.5 as a high-emissions scenario[33]. The study focuses on the evolution of three components of sandy beach shoreline dynamics (Supplementary Fig. 1):

- AC, ambient shoreline dynamics driven by long-term hydrodynamic, geological and anthropic factors;
- *R*, shoreline retreat due to coastal morphological adjustments to SLR;
- *S*, episodic erosion during extreme storms.

The first two components represent longer term shoreline changes and are quantified here as:

$$\mathrm{d}x_{\mathrm{shore,LT}} = \mathrm{AC} + R \quad (1)$$

AC expresses long-term ambient shoreline dynamics that can be driven by a wide range of natural and/or anthropogenic processes, excluding the effect of SLR (*R*) and that of episodic erosion during extreme events (*S*; see following paragraph). In most cases, AC is related to human interventions that alter the sediment budget and/or transport processes of coastal systems[7] but it also includes natural transitions due to a variety of reasons, such as weather patterns[4,34–36], persistent longshore transport variations[37] or geological control[38,39]. *R* in equation (1) represents SLR-driven shoreline retreat, the magnitude of which depends on the amplitude of SLR and the transfer of sediment from the subaerial to the submerged part of the active beach profile, to adjust to rising mean sea levels (MSLs).

The third component *S* represents episodic erosion from intense waves and storm surges during extreme weather events. Episodic erosion is usually followed by a recovery process[40–42]. It is assumed here that the irreversible net effect of episodic erosion and post-storm recovery constitutes part of the ambient shoreline evolution expressed by AC. *S* is therefore limited to the reversible episodic shoreline retreat during storm events relative to its long-term position expressed by $\mathrm{d}x_{\mathrm{shore,LT}}$. Potential variations in storminess with global warming will induce changes in *S* compared to present-day conditions.

At any point in time, the maximum shoreline retreat $\mathrm{d}x_{\mathrm{shore,max}}$ during an extreme coastal event due to the combined effects of long-term and episodic erosion is then defined as:

$$\mathrm{d}x_{\mathrm{shore,max}} = \mathrm{AC} + R + S \quad (2)$$

Each of these components is discussed in more detail below.

This study focuses on ice-free sandy beaches, which constitute the most common and dynamic beach type globally, covering more than 30% of the ice-free coastline in the world[1,43]. While, in reality, shoreline retreat can be limited by the presence of natural or anthropogenic barriers, spatial data on such features are not available globally at the resolution needed for the present study. Adaptive measures against beach erosion could have a similar effect but are difficult to predict and merit a separate study. Therefore, we do not invoke any physical limits to the extent of potential shoreline retreat.

Ambient shoreline dynamics. Several parts of the global coastline undergo long-term ambient changes as a result of various hydrodynamic, geological and anthropic factors. Historical shoreline trends were estimated based on two studies, one by Mentaschi et al.[7] and one by Luijendijk et al.[1]. The former used an updated version of the global surface water (GSW) database[44]. The latter provides spatiotemporal dynamics of surface-water presence globally at 30-m resolution from 1984 to 2015, obtained by the automated analysis of over three million Landsat satellite images. This GSW dataset was processed for changes in water presence in coastal areas to produce time series of cross-shore shoreline position[7]. The pixel-wise information of GSW was translated into cross-shore shoreline dynamics using a set of over 2,000,000 shore-normal transects. The transects were defined every 250 m along a global coastline obtained from OpenStreetMap[45] and were sufficiently long to accommodate the shoreline displacement during the study period. Each transect defines a 200-m shore-wide coastal section, along which surface-water transitions were considered to extract time series of shoreline displacement along each shore-normal transect.

We consider as a proxy for the shoreline change the cross-shore displacement of the seaward boundary of the 'permanent land layer'; that is, the areas where water presence has never been detected throughout the year. Over the 32-yr period considered, the selected proxy can respond to tidal, storm surge, wave and swash dynamics, as well as the inter-related dynamics of the beach-face slope or nearshore bathymetry. Among the different shoreline definitions proposed in literature[46], the present one was chosen as it is more compatible with the type of analysis and the spatial and temporal resolution of the satellite dataset[46]. A detailed description of the procedure, the data and links to the final dataset can be found in Pekel et al.[44] and Mentaschi et al.[7]. Luijendijk et al.[1] used image processing to detect the ocean surface and applied a similar method to the above in order to derive shoreline change rates along transects with an alongshore spacing of 500 m for the world's shoreline.

For the purpose of determining AC in the present study, we consider shoreline dynamics data for a 32-yr period (1984–2015) from updated versions of Luijendijk et al.[1] and Mentaschi et al.[7]. We assume that the time series are representative for present-day ambient shoreline changes and we extrapolate the trend into the future using a probabilistic approach. For each location, we consider the time series of all transects that are within 5 km along the same coastline stretch, using both datasets. This acts as a spatial smoothing to filter out local trends and reflects changes at kilometre scale, which are more relevant in a global-scale analysis. It further ensures that each transect has sufficient data and compensates for gaps in the satellite measurements due to poor quality or lack of data. The original dataset comes with confidence indicators and low-confidence measurements are excluded from the analysis. Similarly, shoreline changes that exceed 5 km in a year are also excluded as outliers.

The above analysis results in sets of annual shoreline displacements for each point, which are sampled randomly to generate synthetic series of future shoreline position with an annual time step. The Monte Carlo sampling results in one million realizations of future shoreline evolution, resulting in probability density functions (PDFs) of annual shoreline displacement during the present century in each transect. The number of realizations was taken to ensure a stable PDF of the shoreline changes by the end the century in all studied transects—that is, when the mean and the standard deviation of the PDFs converged. The realizations of future shoreline evolution assume that ambient change will follow historical trends and express the uncertainty of the historical observations. At certain locations (<2% of the total transects), the detected mean baseline shoreline change trends from Luijendijk et al.[1] and Mentaschi et al.[7] exceed ±10 m yr^{-1}. When such values are extrapolated to the end of the century, this would result in unrealistic values and therefore we limited the mean annual change to ±10 m yr^{-1}.

Shoreline retreat due to SLR. The estimation of the equilibrium shoreline retreat *R* of sandy coasts due to SLR is based on the Bruun rule[18]. This approach builds on the concept that the beach morphology tends to adapt to the prevailing wave climate and is given by:

$$R = \frac{1}{\tan\beta}\mathrm{SLR} \quad (3)$$

where $\tan\beta$ is the active profile slope.

Projections of regional SLR up to the end of this century are available from a probabilistic, process-based approach[47] that combines the major factors contributing to SLR: impact of self-attraction and loading of the ocean upon itself due to the long-term alteration of ocean density changes, globally averaged steric sea-level change, dynamic sea-level change, surface mass balance of ice from glaciers and ice caps, surface mass balance and ice dynamics of Greenland and Antarctic ice sheet, land–water storage and glacial isostatic adjustment. Local smaller scale vertical land movements such as land subsidence due to, for example, groundwater pumping are not included in the SLR projections.

The $\tan\beta$ term in equation (3) expresses the slope of the active beach profile, which to date typically has been assumed to be constant (in space) in large-scale studies[9]. Here, we use a newly released (2019) global dataset of active beach slopes[23]. The dataset has been created combining the MERIT digital elevation dataset[48] with the GEBCO bathymetry[49]. Beach profiles are generated along each sandy beach transect by combining the above bathymetric and topographic data. The offshore boundary of the active profile is defined by the furthest location from the coast with a depth equal to the depth of closure d_c. The latter is calculated using an adaptation of the original Hallermeier[50] formula by Nicholls et al.[51] for applications on longer time scales, given by:

$$d_c = 2.28H_{\mathrm{e}},t - 68.5\left(\frac{H_{\mathrm{e}},t^2}{gT_{\mathrm{e}},t^2}\right) \quad (4)$$

where $H_{\mathrm{e},t}$ is the significant wave height that is exceeded only 12 h per *t* years, $T_{\mathrm{e},t}$ is the associated wave period and *g* is the gravitational acceleration. In this case *t* is equivalent to the 1980–2100 period.

The landward active profile boundary varies among studies and has been defined as the crest of the berm or dune or the most offshore location with an elevation equal to the MSL. In the absence of reliable estimates of the dune or berm height *B*, and following the original definition of the Bruun rule[18] and its application in several recent studies[9,52,53], we take the MSL contour as the landward active profile boundary. The cross-shore distance between these two points is considered as the length of the active profile L_{b}, of which the slope is defined as $\tan\beta = \frac{d_c}{L_b}$.

Waves are simulated over the period 1980 to 2100 using the third-generation spectral wave model WAVEWATCH-III forced by atmospheric conditions from six Coupled Model Intercomparison Project Phase 5 (CMIP5) Global Climate Models (GCMs)[28,54]. The model runs on a global 1.5° grid, combined with several nested finer subgrids with resolution varying from 0.5° to 0.5°. The model's skill to reproduce global wave fields was assessed by comparing time series from a reanalysis covering 35 yr between 1980 and 2014, forced by ERA-Interim wind

data, against altimeter data provided by six different satellites[55]: ERS-2, ENVISAT, Jason 1 and 2, Cryosat 2 and SARAL-AltiKa. Point measurements provided by buoys were used for additional validation. Detailed information on the model set-up and validation can be found in refs. [28,54].

Several recent studies in Australia[41], the Netherlands[56], Spain[57] and France[58] that compared coastline retreat projections obtained via the physics-based probabilistic coastline recession model with those derived with the Bruun rule have indicated that the latter consistently provides higher end estimates of coastline retreat. Acknowledging that the extent of overestimation depends on site-specific factors, we therefore include in our probabilistic framework a correction factor E, which varies randomly between 0.1 and 1.0 centred around a conservative median value 0.75. Thus, here we compute SLR-driven shoreline retreat using the equation:

$$R = E\frac{1}{\tan\beta}\mathrm{SLR} \quad (5)$$

Finally, the active beach slope analysis detected that $\tan\beta$ values in some parts of the world can be as mild as 1/800. According to the Bruun rule and the projected range of SLR, such mild sloping coastal zones will experience shoreline retreats of several hundreds of metres. While not impossible, such estimates could yield serious potential overestimations of real-world shoreline adjustment to SLR[59]. We therefore limit the minimum beach slope to 1/300, which is a realistic lower bound estimate for sandy beaches.

As SLR retreat is estimated in a probabilistic manner through Monte Carlo simulations, the resulting PDFs express the uncertainty from the SLR projections and the Bruun rule error expressed through the E correction factor.

Storm-induced erosion. Episodic erosion during extreme storms is estimated using the convolution erosion model KD93 of Kriebel and Dean[24]. KD93 is based on the equilibrium profile concept and estimates shoreline retreat and volumetric sand loss due to extreme waves and storm surge. KD93 input can be classified in: (1) hydrodynamic variables—significant wave height (H_s), peak wave period (T_p), wave incidence angle (α_w), storm surge (η_s), tidal level (η_{tide}) and event duration; and (2) parameters related to the beach profile—dune height D, berm height B and width W and the beach-face slope $\tan\beta_f$.

Storm surges for the present and future climate conditions are simulated using the DFLOW FM model[60] forced with the same six-member CMIP5 GCMs ensemble as the wave projections[20] (described in the previous section).

The hydrodynamic conditions driving episodic beach erosion are obtained from the wave and storm surge projections. For each of the six GCMs we extracted the storm events simulated during the period 1980–2100, considering the parameters: maximum H_s, η_s, η_{tide} and T_p, as well as mean wave direction Dir_w and event duration. The extraction of storm events is based on the following criteria: (1) maximum H_s or η_s exceeding the 90th percentile value; (2) maximum T_p above 3 s; and (3) maximum H_s above 0.5 m.

The offshore wave conditions are transformed to the nearshore (50-m depth) through wave refraction, shoaling and breaking calculations based on Snell's law, following the approach described in ref. [61]. The wave incidence angle required for the calculations is obtained by combining the wave direction of each event from the model output with the mean shoreline orientation. The active beach slope is obtained from the global dataset mentioned earlier[23].

We then simulate storm-induced erosion for all the above events using KD93 on equilibrium profiles, obtaining a sequence of shoreline retreat events for each transect. Subsequently, we apply non-stationary extreme value statistical analysis[62] and fit a generalized Pareto distribution to the retreat event series to obtain shoreline retreat estimates for different return periods. The present analysis focuses on the storm-induced shoreline retreat for the 100-yr retreat event S_{100} and its difference (ΔS_{100}) compared to present-day conditions.

As storm retreat is estimated in a probabilistic manner through Monte Carlo simulations, the resulting PDFs express the uncertainty from the wave projections (that is, GCM ensemble spread and ocean model error).

Spatial analysis. The study focuses on sandy beaches along the global coastline, which have been detected in a recent study by discretizing the coast at 500-m alongshore transects[1]. We use the Global Human Settlement Layer[63] to estimate the population in low-lying coastal areas (that is, elevation <10 m MSL) within a distance of 25 km from each sandy beach transect. This serves as a proxy for the number of people benefiting from nearby sandy beaches; either receiving natural protection from coastal storms, or benefiting from beach amenity value, or other socioeconomic activities related to tourism, beach-use and so on.

To identify regional patterns in shoreline dynamics, the global coastline is divided in 26 geographical regions (Extended Data Fig. 1), as defined by the IPCC Special Report on Managing the Risks of Extreme Events and Disasters to Advance Climate Change Adaptation (SREX)[64]. The values discussed in the manuscript correspond to averages for each region, country, as well as for the entire global coastline.

Statistical analysis. Equations (1) and (2) are applied here in a probabilistic manner, with the assumption that shoreline change components R, S and AC are independent. PDFs of the three components are combined through Monte Carlo simulations following the steps below[20]: (1) random sampling from the individual PDFs; (2) linear addition of the dx_{shore} components according to equations (1) and (2); (2) control of convergence to ensure that the number of realizations is sufficient; (4) joint PDF estimation. Typically one million realizations are sufficient to obtain stable PDFs and convergence of the final percentiles. The resulting PDF of dx_{shore} expresses the joint contributions from all components and the uncertainty therein (uncertainty factors considered for each component are discussed in previous sections of Methods).

We express the relative contribution of a component by the fraction of its median value to the median total retreat. Similarly, relative contributions to the total dx_{shore} uncertainty is expressed by the fraction of each component's variance to the total variance. We also estimate the difference between the median dx_{shore} values for RCP 4.5 and RCP 8.5.

Limitations. The spatial and temporal scale of the analysis presented here imposes inevitable limitations related to computational resources, data availability and methodological abstraction, the most important of which are discussed next.

Ambient shoreline trends can be an important component of shoreline dynamics and depend on several factors, including the various sediment sources and sinks[57], along with the fate of sediments[65–67]. While smaller scale assessments considered in detail the above factors[68], limitations in terms of modelling capabilities and available datasets, render application of such a methodology at a global scale impossible. Therefore, in the present analysis, we extrapolate historically observed ambient shoreline changes AC into the future, as is common in previous studies[58,69,70]. This is done, however, in a probabilistic way that allows quantifying the temporal variability and inherent uncertainty. As such, future ambient shoreline dynamics follow ongoing trends within uncertainty bounds defined by the spread of the observed historical changes. The 32-yr time window considered may be long enough to express decadal-scale variability in shoreline position but still may not fully resolve some rare cases of coastline change, like those induced by very extreme events or sudden and drastic human interventions. Finally, the 30-m spatial resolution of the satellite dataset may not suffice to resolve smaller displacements in less energetic areas.

Shoreline retreat due to SLR is estimated using the Bruun rule[18], which, despite its known drawbacks, is expected to be adequate for large-scale assessments[9,71]. The Bruun rule is based on the concept that the morphology tends to reach an equilibrium state, which is supported by field observations[40,72,73]. However, the parameterization of the equilibrium profile per se has been a subject of debate[74–76], as the simplified model excludes several factors controlling coastal morphology often found in nature. These include, for example, sediment sinks and sources[68], morphological response to SLR[59], morphological control from natural or artificial structures[6], the presence of nearshore bars[77] or other morphological features[78,79] and longshore processes[65].

Still, despite the criticism[74], the concept is being used extensively because any proposed improvements and modifications[53,80–84] demand data that are often not available. In the present implementation, several of the shortcomings of the Bruun rule are bypassed since R focuses only on what the concept can deliver: that is, alongshore-averaged shoreline response to SLR and changes in wave climate. Most of the factors discussed above and that are beyond the Bruun rule's capacity are expressed by the ambient change AC: for example, changes due to sediment budget imbalances, geological or anthropogenic factors.

The uncertainty related to the active profile slope is another common weakness of the Bruun rule[41], which in the present analysis is addressed through the use of estimates obtained from topobathymetric data. The quantitative accuracy of Bruun rule estimates has also been the subject of rigorous debate for over three decades[41,71,74,85]. Here, we have attempted to address this source of uncertainty by incorporating a correction factor E (equation (5); see also the section Shoreline retreat due to SLR), which is implemented probabilistically within the Monte Carlo framework adopted in our computations.

Beach profile responses to storms are simulated using the KD93 model, rather than with sophisticated process-based models that incorporate elaborate numerical methods and sediment transport modules[86–93]. Such models can potentially provide more accurate estimations of storm erosion (if they are well calibrated and validated), but require as input detailed topobathymetric and sediment grain size information that is not available at a global scale. The present analysis of S required the simulation of about 45 million storm events, rendering the application of models that are computationally more expensive than KD93 practically impossible. In addition, KD93 has produced acceptable results in previous smaller scale applications of similar scope[94–96].

An aspect not covered in our analysis is the effect of storm clusters. It has been discussed extensively in previous studies, based either on field data[40,42] or numerical models[86,97–99], that storm chronology can enhance the impact of individual events. These studies have also shown that storm erosion can be followed by beach recovery. The last is a complex process that is difficult to simulate[72,100] and requires in situ data. Predicting the maximum erosion from storm clusters at a global scale is therefore a challenging task. We consider only the episodic erosion from individual storms without accounting for storm groups and do not simulate post-storm recovery. Rather it is assumed that the combined, long-term, residual effects of erosion and recovery are included in the ambient change component AC.

The present analysis assumes unlimited backshore space for shoreline retreat. Some natural coastal systems may have such accommodation space, while in

other sites this may be strongly limited by human development or physical barriers. This is a known issue which combined with SLR can have societal and ecological implications discussed in the literature, especially under the term of coastal squeeze[101,102]. In principle, satellite imagery could provide formation on beach width[103] and available space for coastal retreat at the backshore, yet such a global dataset is not available. Socioeconomic projections suggest that coastal development will probably continue in the decades to come[12,13], which may further reduce the accommodating space for coastal retreat. We consider arbitrary erosion threshold values to indicate potential changes that could be critical for sandy beaches. With the information on backshore space and development that may be available at local/regional scales, our publicly available projections could be used by scientists and practitioners to carry out more detailed smaller scale assessments.

Additional results. *SLR retreat.* Rising sea levels will result in shoreline retreat along the entire global coastline with the exception of a few regions that experience uplift, like the Baltic Sea (Extended Data Fig. 2). The global average median *R* by 2050 (relative to 2010) is projected to be around −28 m and −35 m under RCP 4.5 and RCP 8.5, respectively. By the end of the century, SLR-driven erosion is projected to further grow to around −63 m and −105 m, respectively. The retreat of sandy beaches due to SLR is projected to be highest (at least 130 m by 2100 relative to 2010 under RCP 8.5) in North Australia, central North America, northeast Brazil, South and Southeast Asia and central Europe. Other regions for which high *R* values are projected include West Africa, southeastern South America, South Australia/New Zealand, East Asia and eastern North America.

Ambient changes. The present section discusses long-term ambient changes as a result of hydrodynamic, geological and anthropic factors. The global averaged AC is erosive, corresponding to global average land retreat of −10.4 m by 2050 (probable range between −33.7 and 12.8 m) and of −23.5 m by the end of the century (probable range between −72.2 and 25.2 m). The stronger erosion is projected for South Asia, the Caribbean SIDS, central North America and southeastern South America with the probable range by the end of the century being from −282.3 to −88.7 m, from −160 to −84.3, from −116.8 to −44.9 m and from −143.6 to −10.3 m, respectively (Extended Data Fig. 3). East Asia shows a strong accretive ambient shoreline change trend (very likely range: 112.3–173.2 m), being the result of major coastal land reclamations over the recent decades.

Smaller scale projections show high spatial variability with erosive and accretive trends interchanging. Examples of accretion hotspots in Central America/Mexico can be found in Colombia, both on the Caribbean Sea and on the Pacific Ocean, especially at the mouths of the rivers Atrato, Sinu, Magdalena, Jurubida, San Juan and others. In central North America, the long-term trends of coastal erosion/accretion are dominated by the dynamics at the mouth of the Mississippi river. The area is very dynamic, with large erosive spots (for example, the Terrebonne Bay) and accretive spots (for example, the Atchafalaya delta[104]). Furthermore, the area is frequently hit by tropical cyclones[105] that may cause abrupt extreme erosion, for example, hurricane Katrina, the largest natural disaster in the history of the United States[106] and hurricane Rita in 2005.

In northeast Brazil, the activity is dominated by the morphodynamics of the Tocantins delta and along the coasts of Para–Maranhao–Piaui–Ceara, a very active area characterized by both extreme coastal erosion and accretion[7]. The dominance of accretion is probably due to the erosivity of the soil in the interior, a rich river network that transports sediments towards the sea and strong macro-tidal currents carrying them along the coasts[107].

The most active areas in southern Africa are the coasts of Mozambique and the western coasts of Madagascar, areas characterized by intense tidal currents. Accretion prevails especially in Madagascar, probably due to internal erosion and subsequent transport of sediment towards the coasts, and redistribution of it by currents[108].

Southeast Asia is characterized by both extreme erosion and accretion. Intense erosion can be observed, for example, at the deltas of the rivers Sittaung[109] and Mekong[19] or in areas of strong land subsidence, like the northern coast of Java[110] or in the northern Manila Bay[111]. Examples of areas dominated by extreme accretion are the extended delta of the Red River in North Vietnam, western New Guinea, several river deltas in the Malaysian peninsula and Sumatra, as well as in intensely built sites such as Bangkok and Singapore. A more detailed discussion on the local/regional variations can be found in Mentaschi et al.[7].

Data availability

The models and datasets presented are part of the integrated risk assessment tool LISCoAsT (Large scale Integrated Sea-level and Coastal Assessment Tool) developed by the Joint Research Centre of the European Commission. The dataset is available through the LISCoAsT repository of the JRC data collection: http://data.europa.eu/89h/18eb5f19-b916-454f-b2f5-88881931587e.

Code availability

The code that supported the findings of this study is available from the corresponding author upon reasonable request.

References

33. Meinshausen, M. et al. The RCP greenhouse gas concentrations and their extensions from 1765 to 2300. *Clim. Change* **109**, 213–241 (2011).
34. Hurst, M. D., Rood, D. H., Ellis, M. A., Anderson, R. S. & Dornbusch, U. Recent acceleration in coastal cliff retreat rates on the south coast of Great Britain. *Proc. Natl Acad. Sci. USA* **113**, 13336–13341 (2016).
35. Ruggiero, P. Is the intensifying wave climate of the U.S. Pacific Northwest increasing flooding and erosion risk faster than sea-level rise? *J. Waterw. Port Coast. Ocean Eng.* **139**, 88–97 (2013).
36. Loureiro, C., Ferreira, Ó. & Cooper, J. A. G. Extreme erosion on high-energy embayed beaches: influence of megarips and storm grouping. *Geomorphology* **139–140**, 155–171 (2012).
37. Kroon, A. et al. Statistical analysis of coastal morphological data sets over seasonal to decadal time scales. *Coast. Eng.* **55**, 581–600 (2008).
38. Gallop, S. L., Bosserelle, C., Pattiaratchi, C. & Eliot, I. Rock topography causes spatial variation in the wave, current and beach response to sea breeze activity. *Mar. Geol.* **290**, 29–40 (2011).
39. Vousdoukas, M. I., Velegrakis, A. F. & Plomaritis, T. A. Beachrock occurrence, characteristics, formation mechanisms and impacts. *Earth Sci. Rev.* **85**, 23–46 (2007).
40. Vousdoukas, M. I., Almeida, L. P. & Ferreira, Ó. Beach erosion and recovery during consecutive storms at a steep-sloping, meso-tidal beach. *Earth Surf. Process. Landf.* **37**, 583–691 (2012).
41. Ranasinghe, R., Callaghan, D. & Stive, M. J. F. Estimating coastal recession due to sea level rise: beyond the Bruun rule. *Clim. Change* **110**, 561–574 (2012).
42. Coco, G. et al. Beach response to a sequence of extreme storms. *Geomorphology* **204**, 493–501 (2014).
43. Hardisty, J. in *Sediment Transport and Depositional Processes* (Ed. Pye, K.) 216–255 (Blackwell, 1994).
44. Pekel, J.-F., Cottam, A., Gorelick, N. & Belward, A. S. High-resolution mapping of global surface water and its long-term changes. *Nature* **540**, 418–422 (2016).
45. Haklay, M. & Weber, P. OpenStreetMap: user-generated street maps. *IEEE Pervasive Comput.* **7**, 12–18 (2008).
46. Boak, E. H. & Turner, I. L. Shoreline definition and detection: a review. *J. Coast. Res.* **21**, 688–703 (2005).
47. Jackson, L. P. & Jevrejeva, S. A probabilistic approach to 21st century regional sea-level projections using RCP and high-end scenarios. *Glob. Planet. Change* **146**, 179–189 (2016).
48. Yamazaki, D. et al. A high-accuracy map of global terrain elevations. *Geophys. Res. Lett.* **44**, 5844–5853 (2017).
49. Weatherall, P. et al. A new digital bathymetric model of the world's oceans. *Earth Space Sci.* **2**, 331–345 (2015).
50. Hallermeier, R. J. Uses for a calculated limit depth to beach erosion. In *Proc. 16th International Conference on Coastal Engineering* 1493–1512 (American Society of Civil Engineers, 1978).
51. Nicholls, R. J., Birkemeier, W. A. & Lee, G.-h Evaluation of depth of closure using data from Duck, NC, USA. *Mar. Geol.* **148**, 179–201 (1998).
52. Baron, H. M. et al. Incorporating climate change and morphological uncertainty into coastal change hazard assessments. *Nat. Hazards* **75**, 2081–2102 (2015).
53. Ranasinghe, R., Duong, T. M., Uhlenbrook, S., Roelvink, D. & Stive, M. Climate-change impact assessment for inlet-interrupted coastlines. *Nat. Clim. Change* **3**, 83–87 (2012).
54. Vousdoukas, M. I., Mentaschi, L., Voukouvalas, E., Verlaan, M. & Feyen, L. Extreme sea levels on the rise along Europe's coasts. *Earth's Future* https://doi.org/10.1002/2016EF000505 (2017).
55. Queffeulou, P. & Croizé-Fillon, D. *Global Altimeter SWH Dataset* (Laboratoire d'Océanographie Spatiale, IFREMER, 2014).
56. Li, F. *Probabilistic Estimation of Dune Erosion and Coastal Zone Risk*. PhD thesis, Delft Univ. Technology (2014).
57. Toimil, A., Losada, I. J., Camus, P. & Díaz-Simal, P. Managing coastal erosion under climate change at the regional scale. *Coast. Eng.* **128**, 106–122 (2017).
58. Le Cozannet, G. et al. Quantifying uncertainties of sandy shoreline change projections as sea level rises. *Sci. Rep.* **9**, 42 (2019).
59. Lentz, E. E. et al. Evaluation of dynamic coastal response to sea-level rise modifies inundation likelihood. *Nat. Clim. Change* **6**, 696–700 (2016).
60. Muis, S., Verlaan, M., Winsemius, H. C., Aerts, J. C. J. H. & Ward, P. J. A global reanalysis of storm surges and extreme sea levels. *Nat. Commun.* **7**, 11969 (2016).
61. *Coastal Engineering Manual* Part II, Ch. 2 (US Army Corps of Engineers, 2002).
62. Mentaschi, L. et al. Non-stationary extreme value analysis: a simplified approach for earth science applications. *Hydrol. Earth Syst. Sci. Discuss.* **2016**, 1–38 (2016).
63. Corbane, C. et al. Big earth data analytics on Sentinel-1 and Landsat imagery in support to global human settlements mapping. *Big Earth Data* **1**, 118–144 (2017).
64. IPCC (eds Field, C. B. et al.) *Managing the Risks of Extreme Events and Disasters to Advance Climate Change Adaptation* (Cambridge Univ. Press, 2012).

65. Antolínez, J. A. A. et al. A multiscale climate emulator for long-term morphodynamics (MUSCLE-morpho). *J. Geophys. Res. Oceans* **121**, 775–791 (2016).
66. Enríquez, A. R., Marcos, M., Álvarez-Ellacuría, A., Orfila, A. & Gomis, D. Changes in beach shoreline due to sea level rise and waves under climate change scenarios: application to the Balearic Islands (western Mediterranean). *Nat. Hazards Earth Syst. Sci.* **17**, 1075–1089 (2017).
67. Anderson, D., Ruggiero, P., Antolínez, J. A. A., Méndez, F. J. & Allan, J. A climate index optimized for longshore sediment transport reveals interannual and multidecadal littoral cell rotations. *J. Geophys. Res. Earth Surf.* **123**, 1958–1981 (2018).
68. Giardino, A. et al. A quantitative assessment of human interventions and climate change on the West African sediment budget. *Ocean Coast. Manag.* **156**, 249–265 (2018).
69. Vitousek, S., Barnard, P. L., Limber, P., Erikson, L. & Cole, B. A model integrating longshore and cross-shore processes for predicting long-term shoreline response to climate change. *J. Geophys. Res. Earth Surf.* **122**, 782–806 (2017).
70. Wainwright, D. J. et al. Moving from deterministic towards probabilistic coastal hazard and risk assessment: development of a modelling framework and application to Narrabeen Beach, New South Wales, Australia. *Coast. Eng.* **96**, 92–99 (2015).
71. Ranasinghe, R. & Stive, M. J. F. Rising seas and retreating coastlines. *Clim. Change* **97**, 465 (2009).
72. Davidson, M. A., Splinter, K. D. & Turner, I. L. A simple equilibrium model for predicting shoreline change. *Coast. Eng.* **73**, 191–202 (2013).
73. Ozkan-Haller, T. & Brundidge, S. Equilibrium beach profiles for Delaware beaches. *J. Waterw. Port Coast. Ocean Eng* . **133**, 147–160 (2007).
74. Cooper, J. A. G. & Pilkey, O. H. Sea-level rise and shoreline retreat: time to abandon the Bruun Rule. *Glob. Planet. Change* **43**, 157–171 (2004).
75. Pilkey, O. H. & Dixon, K. L. *The Corps and the Shore* (Island Press, 1996).
76. Pilkey, O. H. et al. The concept of shoreface profile of equilibrium: a critical review. *J. Coast. Res.* **9**, 225–278 (1993).
77. Holman, R. A., Lalejini, D. M., Edwards, K. & Veeramony, J. A parametric model for barred equilibrium beach profiles. *Coast. Eng.* **90**, 85–94 (2014).
78. Coco, G. & Murray, A. B. Patterns in the sand: from forcing templates to self-organization. *Geomorphology* **91**, 271–290 (2007).
79. Vousdoukas, M. I. Erosion/accretion and multiple beach cusp systems on a meso-tidal, steeply-sloping beach. *Geomorphology* **141–142**, 34–46 (2012).
80. Wang, Z. & Dean, R. G. in *Coastal Sediments '07* (eds Kraus, N. C. & Rosati, J. D.) 626–632 (American Society of Civil Engineers, 2007).
81. Dai, Z.-J., Du, J.-z, Li, C.-C. & Chen, Z.-S. The configuration of equilibrium beach profile in South China. *Geomorphology* **86**, 441–454 (2007).
82. Romanczyk, W., Boczar-Karakiewicz, B. & Bona, J. L. Extended equilibrium beach profiles. *Coast. Eng.* **52**, 727–744 (2005).
83. Anderson, T. R., Fletcher, C. H., Barbee, M. M., Frazer, L. N. & Romine, B. M. Doubling of coastal erosion under rising sea level by mid-century in Hawaii. *Nat. Hazards* **78**, 75–103 (2015).
84. Bray, M. & Hooke, J. Prediction of soft-cliff retreat with accelerating sea-level rise. *J. Coast. Res.* **13**, 453–467 (1997).
85. Pilkey, O. H. & Cooper, J. A. G. Society and sea level rise. *Science* **303**, 1781 (2004).
86. Splinter, K. D., Carley, J. T., Golshani, A. & Tomlinson, R. A relationship to describe the cumulative impact of storm clusters on beach erosion. *Coast. Eng.* **83**, 49–55 (2014).
87. Vousdoukas, M. I., Ferreira, O., Almeida, L. P. & Pacheco, A. Toward reliable storm-hazard forecasts: XBeach calibration and its potential application in an operational early-warning system. *Ocean Dyn.* **62**, 1001–1015 (2012).
88. Roelvink, D. et al. Modelling storm impacts on beaches, dunes and barrier islands. *Coast. Eng.* **56**, 1133–1152 (2009).
89. Broekema, Y. B. et al. Observations and modelling of nearshore sediment sorting processes along a barred beach profile. *Coast. Eng.* **118**, 50–62 (2016).
90. de Winter, R. C. & Ruessink, B. G. Sensitivity analysis of climate change impacts on dune erosion: case study for the Dutch Holland coast. *Clim. Change* **141**, 685–701 (2017).
91. Karunarathna, H., Brown, J., Chatzirodou, A., Dissanayake, P. & Wisse, P. Multi-timescale morphological modelling of a dune-fronted sandy beach. *Coast. Eng.* **136**, 161–171 (2018).
92. Passeri, D. L., Bilskie, M. V., Plant, N. G., Long, J. W. & Hagen, S. C. Dynamic modeling of barrier island response to hurricane storm surge under future sea level rise. *Clim. Change* **149**, 413–425 (2018).
93. Vousdoukas, M. I. et al. *Proc. 11th International Coastal Symposium* (Coastal Education & Research Foundation, Inc., 2011).
94. Callaghan, D. P., Nielsen, P., Short, A. D. & Ranasinghe, R. Statistical simulation of wave climate and extreme beach erosion. *Coast. Eng.* **55**, 375–390 (2008).
95. Ferreira, Ó., Garcia, T., Matias, A., Taborda, R. & Dias, J. A. An integrated method for the determination of set-back lines for coastal erosion hazards on sandy shores. *Continent. Shelf Res.* **26**, 1030–1044 (2006).
96. Mull, J. & Ruggiero, P. Estimating storm-induced dune erosion and overtopping along U.S. West Coast beaches. *J. Coast. Res.* **30**, 1173–1187 (2014).
97. Ferreira, Ó. Storm groups versus extreme single storms: predicted erosion and management consequences. *J. Coast. Res.* **42**, 155–161 (2005).
98. Dissanayake, P., Brown, J. & Karunarathna, H. Impacts of storm chronology on the morphological changes of the formby beach and dune system, UK. *Nat. Hazards Earth Syst. Sci.* **3**, 2565–2597 (2015).
99. Hackney, C., Darby, S. E. & Leyland, J. Modelling the response of soft cliffs to climate change: a statistical, process-response model using accumulated excess energy. *Geomorphology* **187**, 108–121 (2013).
100. Yates, M. L., Guza, R. T. & O'Reilly, W. C. Equilibrium shoreline response: observations and modeling. *J. Geophys. Res.* **114**, C09014 (2009).
101. Pontee, N. Defining coastal squeeze: a discussion. *Ocean Coast. Manag.* **84**, 204–207 (2013).
102. Doody, J. P. Coastal squeeze and managed realignment in southeast England, does it tell us anything about the future? *Ocean Coast. Manag.* **79**, 34–41 (2013).
103. Monioudi, I. N. et al. Assessment of island beach erosion due to sea level rise: the case of the Aegean archipelago (Eastern Mediterranean). *Nat. Hazards Earth Syst. Sci.* **17**, 449–466 (2017).
104. Rosen, T. & Xu, Y. J. Recent decadal growth of the Atchafalaya river delta complex: effects of variable riverine sediment input and vegetation succession. *Geomorphology* **194**, 108–120 (2013).
105. Peduzzi, P. et al. Global trends in tropical cyclone risk. *Nat. Clim. Change* **2**, 289–294 (2012).
106. Travis, J. Scientists fears come true as hurricane floods New Orleans. *Science* **309**, 1656 (2005).
107. Monteiro, M. C., Pereira, L. C. C. & de Oliveira, S. M. O. Morphodynamic changes of a macrotidal sand beach in the Brazilian Amazon Coast (Ajuruteua-Pará). *J. Coast. Res.* **SI56**, 103–107 (2009).
108. Salomon, J.-N. L'accrétion littorale sur la côte Ouest de Madagascar. *Physio-Géo* **3**, 35–59 (2009).
109. Taft, L. & Evers, M. A review of current and possible future human–water dynamics in myanmar's river basins. *Hydrol. Earth Syst. Sci.* **20**, 4913–4928 (2016).
110. Marfai, M. A. & King, L. Monitoring land subsidence in Semarang, Indonesia. *Environ. Geol.* **53**, 651–659 (2007).
111. Rodolfo, K. S. & Siringan, F. P. Global sea-level rise is recognised, but flooding from anthropogenic land subsidence is ignored around northern Manila Bay, Philippines. *Disasters* **30**, 118–139 (2006).

Acknowledgements

R.R. is supported by the AXA Research fund and the Deltares Strategic Research Programme 'Coastal and Offshore Engineering'. P.A. is supported by the EU Horizon 2020 Programme for Research and Innovation under grant no. 776613 (EUCP: European Climate Prediction system). T.P. was funded by the research group RNM-328 of the Andalusian Research Plan (PAI) and the Portuguese Science and Technology Foundation (FCT) through grant no. UID/MAR/00350/2013 attributed to CIMA of the University of Algarve. The authors are grateful to A. Giardino and A. van Dongeren for providing helpful comments on the manuscript and the methodology, and E. Voukouvalas for contributing to the generation of the storm surge dataset.

Author contributions

M.I.V, R.R. and L.F. jointly conceived the study. M.I.V. and L.M. produced the storm surge and wave projections. L.M. produced the ambient shoreline change data and developed the extreme value statistical analysis methodology. M.I.V. and T.A.P. produced the storm erosion and SLR retreat projections. P.A. produced the global beach slope dataset. A.L. produced the global sandy beach presence dataset. M.I.V. analysed the data and prepared the manuscript, with all authors discussing results and implications and commenting on the manuscript at all stages.

Competing interests

The authors declare no competing interests.

Additional information

Extended data is available for this paper at https://doi.org/10.1038/s41558-020-0697-0.

Supplementary information is available for this paper at https://doi.org/10.1038/s41558-020-0697-0.

Correspondence and requests for materials should be addressed to M.I.V.

Peer review information *Nature Climate Change* thanks Patrick Barnard, Mark Davidson and the other, anonymous, reviewer(s) for their contribution to the peer review of this work.

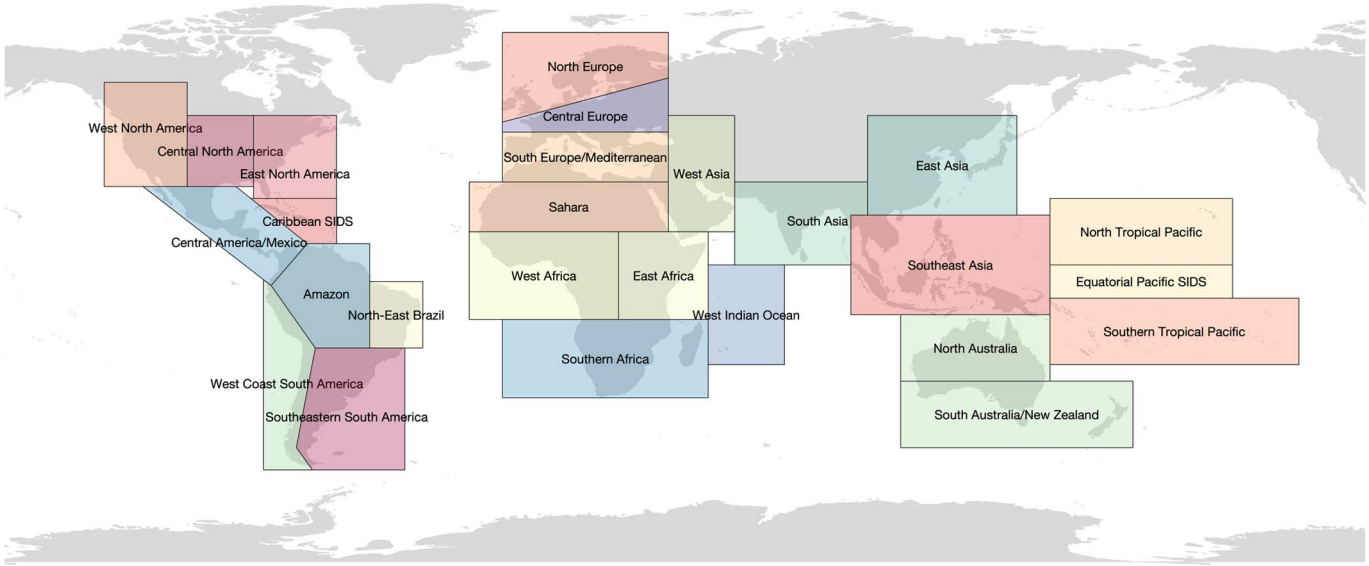

Extended Data Fig. 1 | Geographical regions considered in the present analysis. Geographical regions considered in the present analysis, based on the IPCC SREX report and limited to those that contain ice-free sandy coastlines.

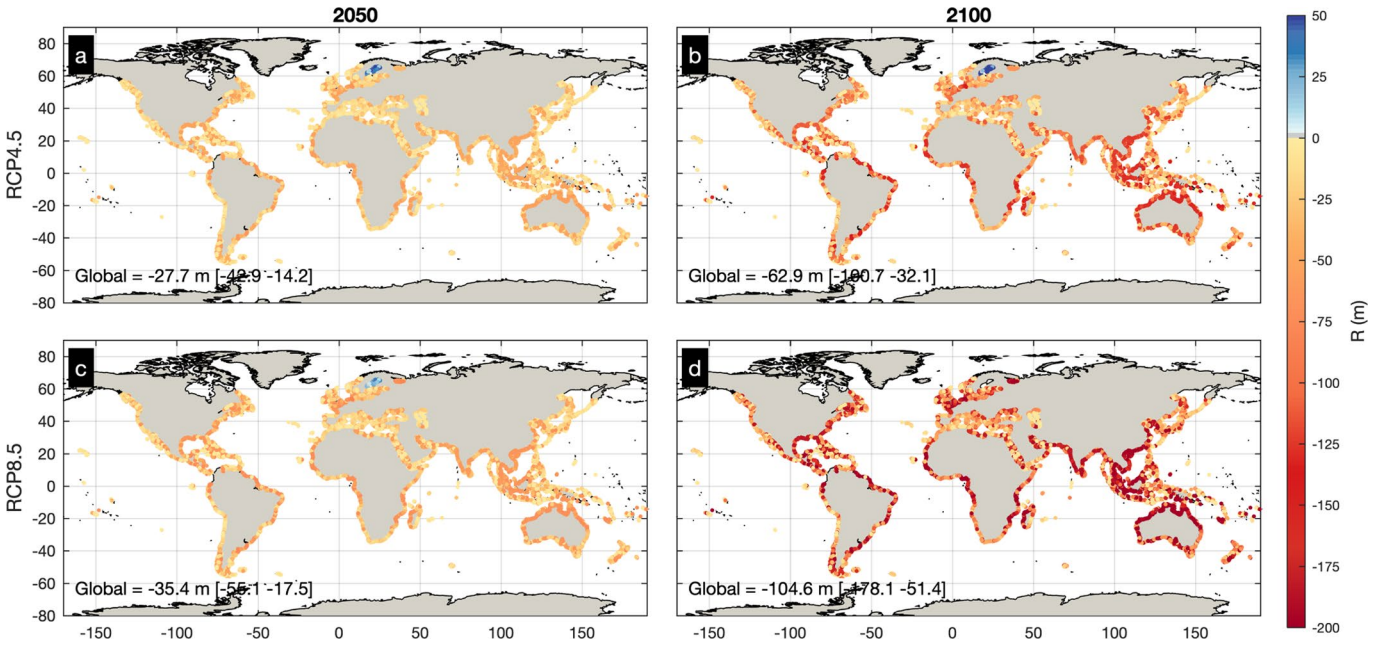

Extended Data Fig. 2 | Projected long-term shoreline change due to SLR-driven retreat (R) alone, by the year 2050 and 2100 under RCP4.5 and RCP8.5. Projected long-term shoreline change due to SLR-driven retreat (R) alone, by the year 2050 (a,c) and 2100 (b,d) under RCP4.5 (a-b) and RCP8.5 (c-d). Values represent the median change and positive/negative values express accretion/erosion in m, relative to 2010. The global average median change is shown in the inset text for each case, along with the 5th-95th percentile range.

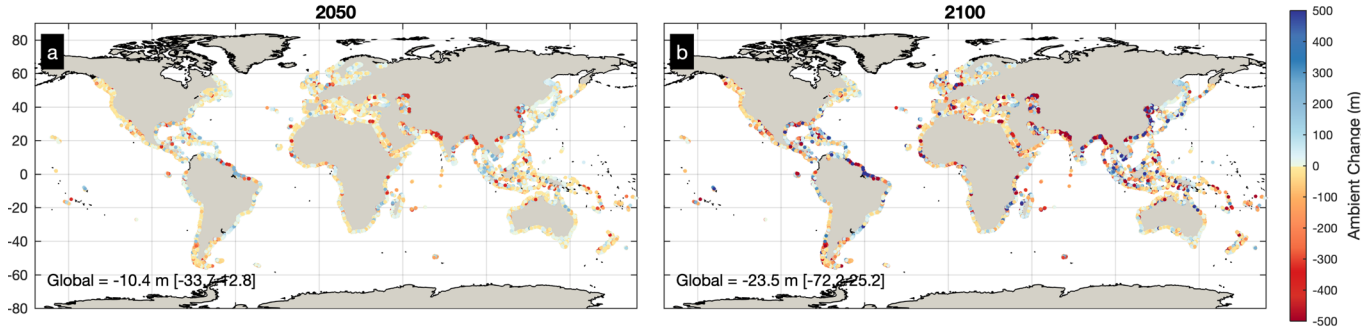

Extended Data Fig. 3 | Projected long-term shoreline change driven due to the ambient shoreline change rate (AC) alone, by the year 2050 and 2100. Projected long-term shoreline change driven due to the ambient shoreline change rate (AC) alone, by the year 2050 (a) and 2100 (b). Values represent the median change and positive/negative values express accretion/erosion in m, relative to 2010. The global average median change is shown in the inset text for each case, along with the 5th-95th percentile range.

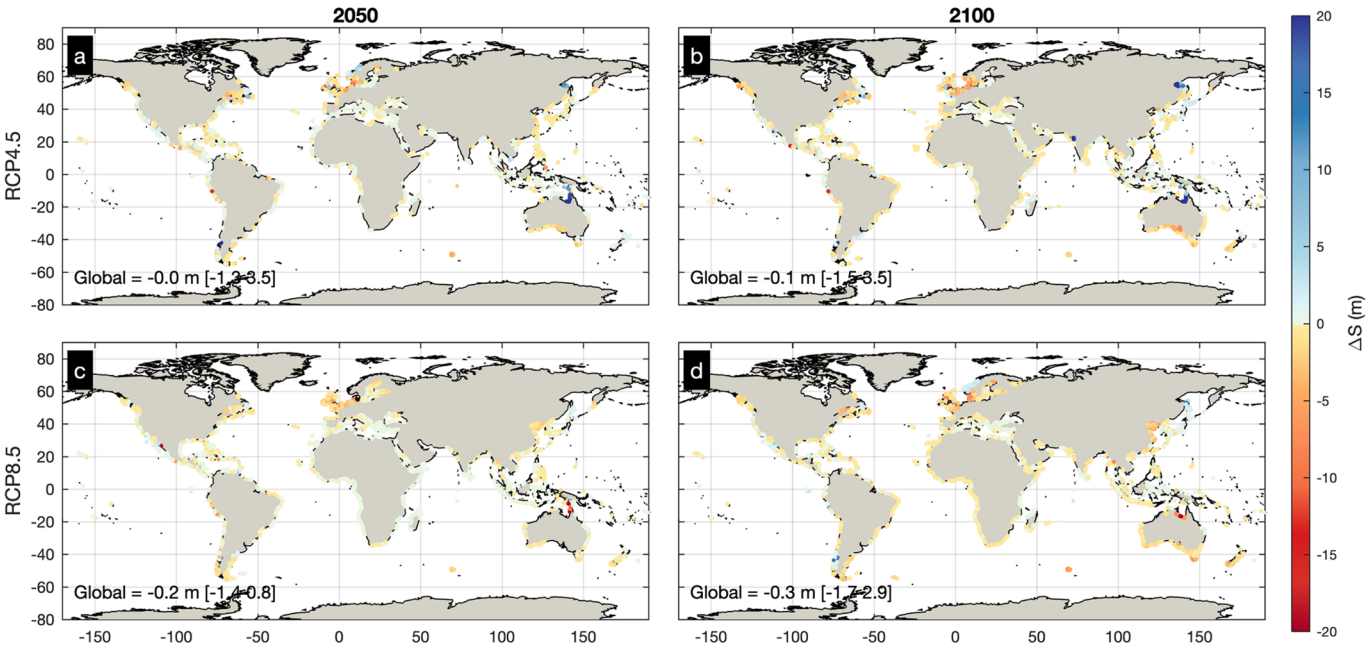

Extended Data Fig. 4 | Projected change in 100-year episodic beach erosion for the year 2050 and 2100 under RCP4.5 and RCP8.5. Projected change in 100-year episodic beach erosion for the year 2050 (a,c) and 2100 (b,d) under RCP4.5 (a-b) and RCP8.5 (c-d). Values represent the median change and positive/negative values express less/more erosion (m), relative to 2010. The global average median change is shown in the inset text for each case, along with the 5th-95th percentile range.

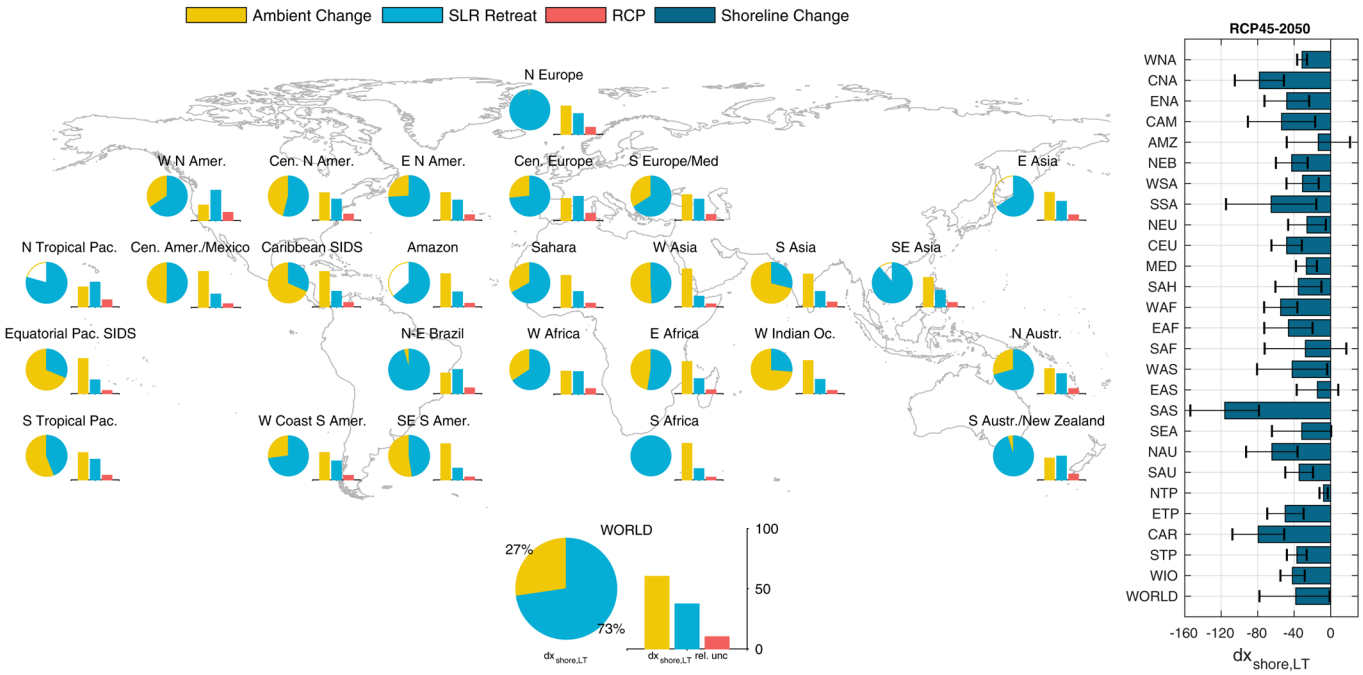

Extended Data Fig. 5 | Projected median long-term shoreline change under RCP4.5 by the year 2050 ($dx_{shore,LT}$), for the 26 IPCC SREX sub-regions and the worldwide average. Projected median long-term shoreline change under RCP4.5 by the year 2050 ($dx_{shore,LT}$), for the 26 IPCC SREX sub-regions and the worldwide average (horizontal bar plot; positive/negative values express accretion/erosion in m). Shoreline change is considered to be the result of SLR retreat (R) and ambient shoreline change trends (AC). Pie plots show the relative contributions of R and AC to the projected median $dx_{shore,LT}$, with transparent patches expressing accretive trends. Vertical bar plots show the relative contributions of R and AC, as well as that of RCPs, to the total uncertainty in projected median $dx_{shore,LT}$.

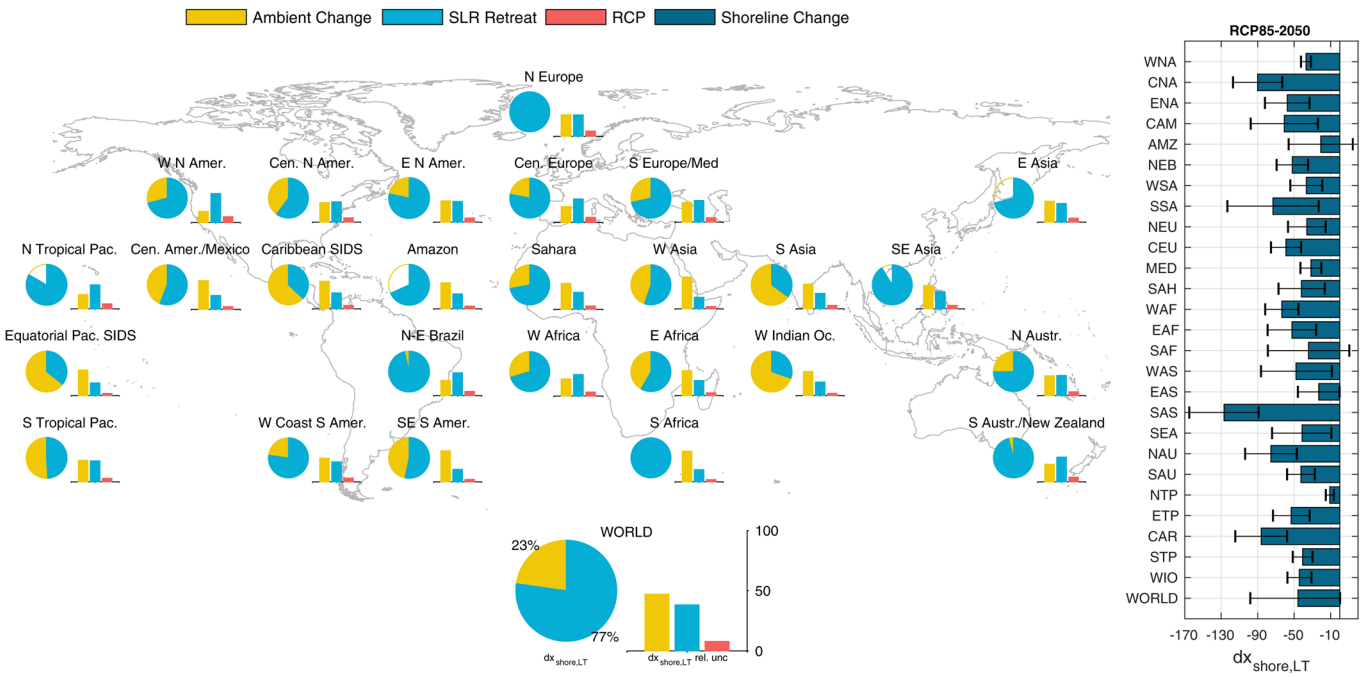

Extended Data Fig. 6 | Projected median long-term shoreline change under RCP8.5 by the year 2050 ($dx_{shore,LT}$), for the 26 IPCC SREX sub-regions and the worldwide average. Projected median long-term shoreline change under RCP8.5 by the year 2050 ($dx_{shore,LT}$), for the 26 IPCC SREX sub-regions and the worldwide average (horizontal bar plot; positive/negative values express accretion/erosion in m). Shoreline change is considered to be the result of SLR retreat (R) and ambient shoreline change trends (AC). Pie plots show the relative contributions of R and AC to the projected median $dx_{shore,LT}$, with transparent patches expressing accretive trends. Vertical bar plots show the relative contributions of R and AC, as well as that of RCPs, to the total uncertainty in projected median $dx_{shore,LT}$.

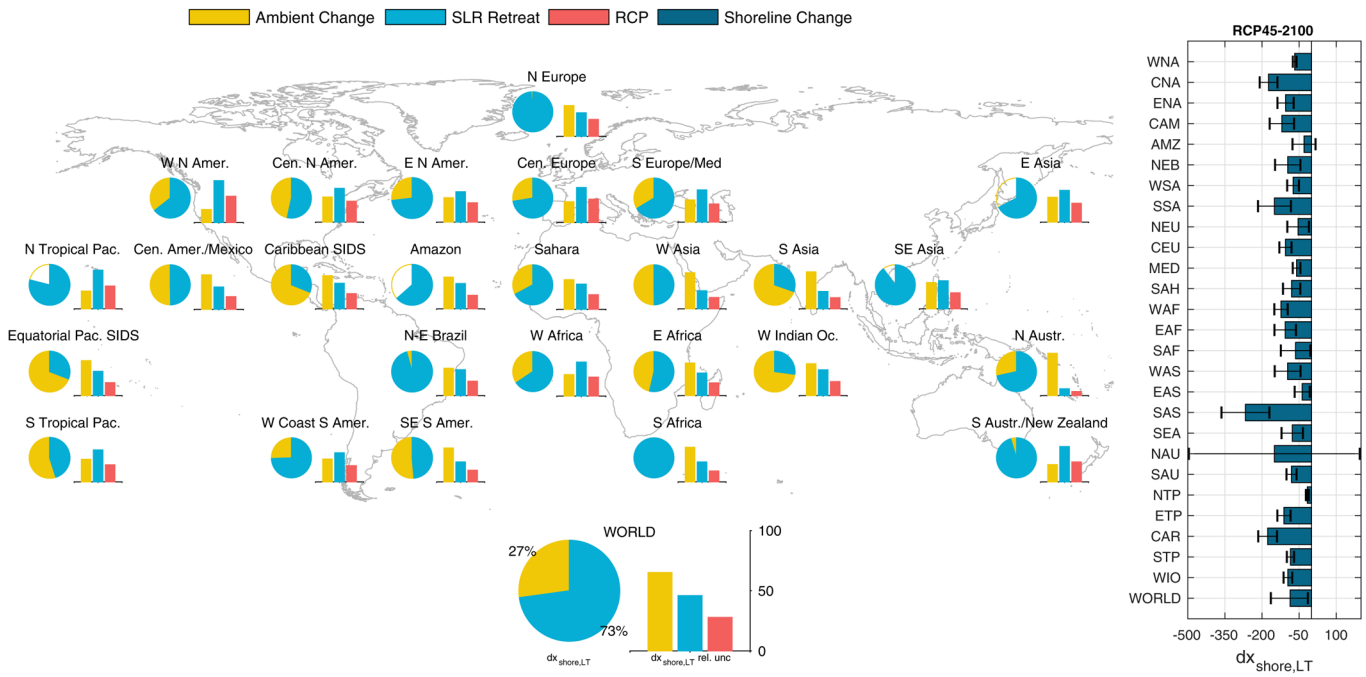

Extended Data Fig. 7 | Projected median long-term shoreline change under RCP4.5 by the year 2100 ($dx_{shore,LT}$), for the 26 IPCC SREX sub-regions and the worldwide average. Projected median long-term shoreline change under RCP4.5 by the year 2100 ($dx_{shore,LT}$), for the 26 IPCC SREX sub-regions and the worldwide average (horizontal bar plot; positive/negative values express accretion/erosion in m). Shoreline change is considered to be the result of SLR retreat (R) and ambient shoreline change trends (AC). Pie plots show the relative contributions of R and AC to the projected median $dx_{shore,LT}$, with transparent patches expressing accretive trends. Vertical bar plots show the relative contributions of R and AC, as well as that of RCPs, to the total uncertainty in projected median $dx_{shore,LT}$.

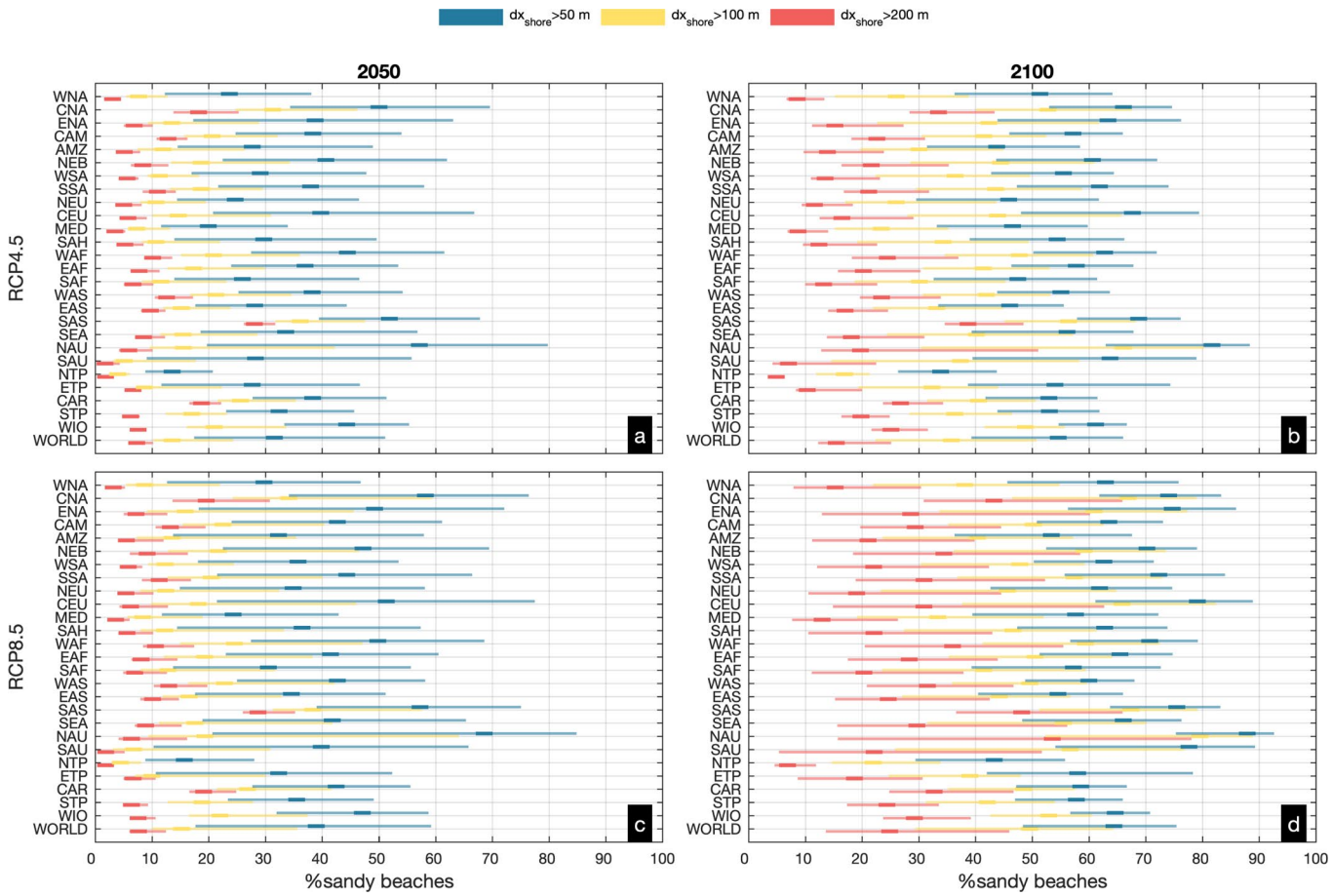

Extended Data Fig. 8 | Percentage length of sandy beach shoreline that is projected to retreat by more than 50, 100 and 200 m per IPCC SREX sub-region. Bar plots showing, per IPCC SREX sub-region, the percentage length of sandy beach shoreline that is projected to retreat by more than 50 (blue), 100 (yellow) and 200 m (red), by 2050 (a,c) and 2100 (b,d), under RCP4.5 (a-b) and RCP8.5 (c-d) relative to 2010. Transparent colour patches indicate the 5th-95th quantile range and solid rectangles show the median value. For the region abbreviations, please see Extended Data Fig. 1.

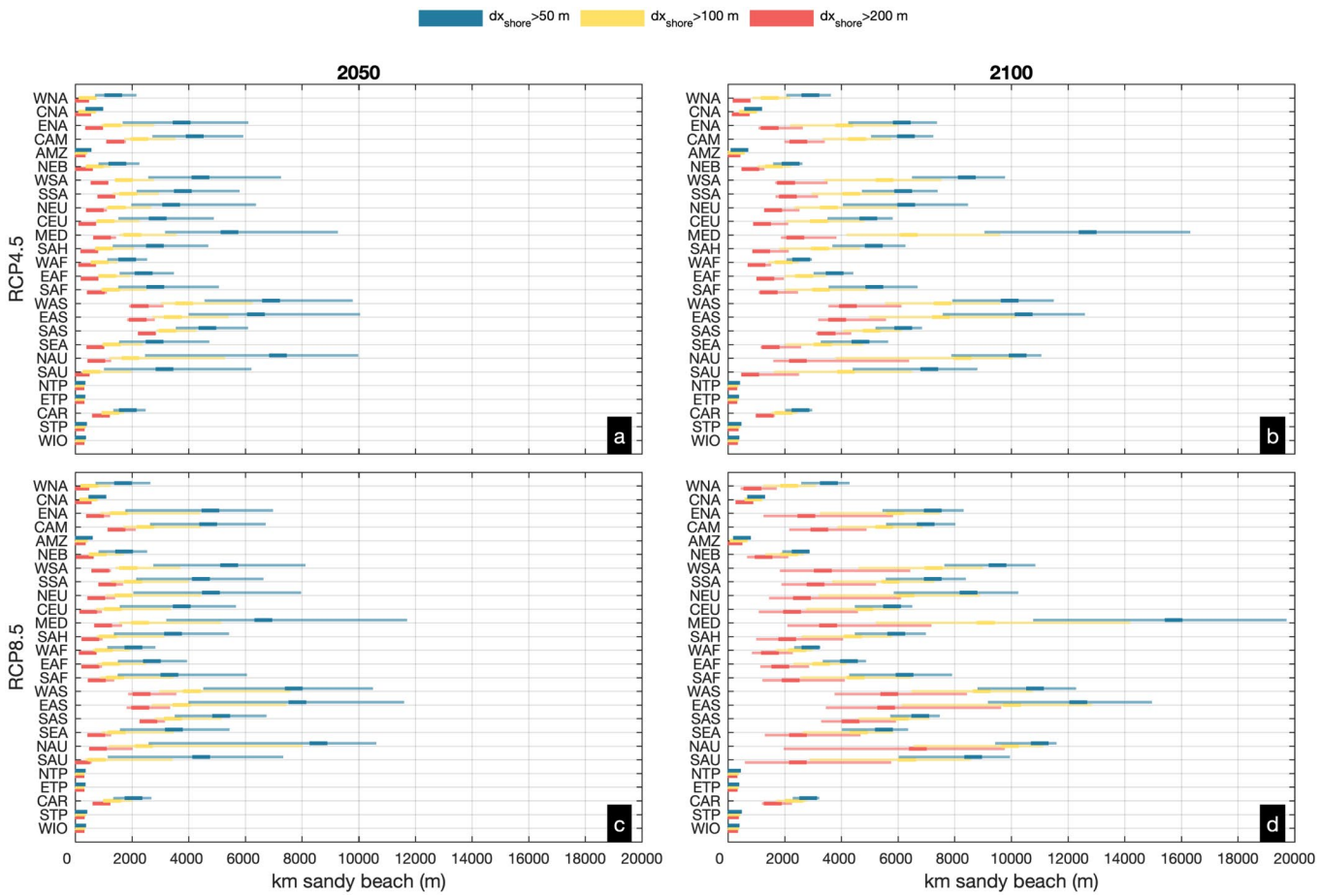

Extended Data Fig. 9 | Length of sandy beach shoreline that is projected to retreat by more than 50, 100 and 200 m per IPCC SREX sub-region. Bar plots showing, per IPCC SREX sub-region, the length (in km) of sandy beach shoreline that is projected to retreat by more than 50 (blue), 100 (yellow) and 200 m (red), by 2050 (a,c) and 2100 (b,d), under RCP4.5 (a-b) and RCP8.5 (c-d) relative to 2010. Transparent colour patches indicate the 5th-95th quantile range and solid rectangles show the median value. For the region abbreviations, please see Supplementary Figs. 2 and 5.

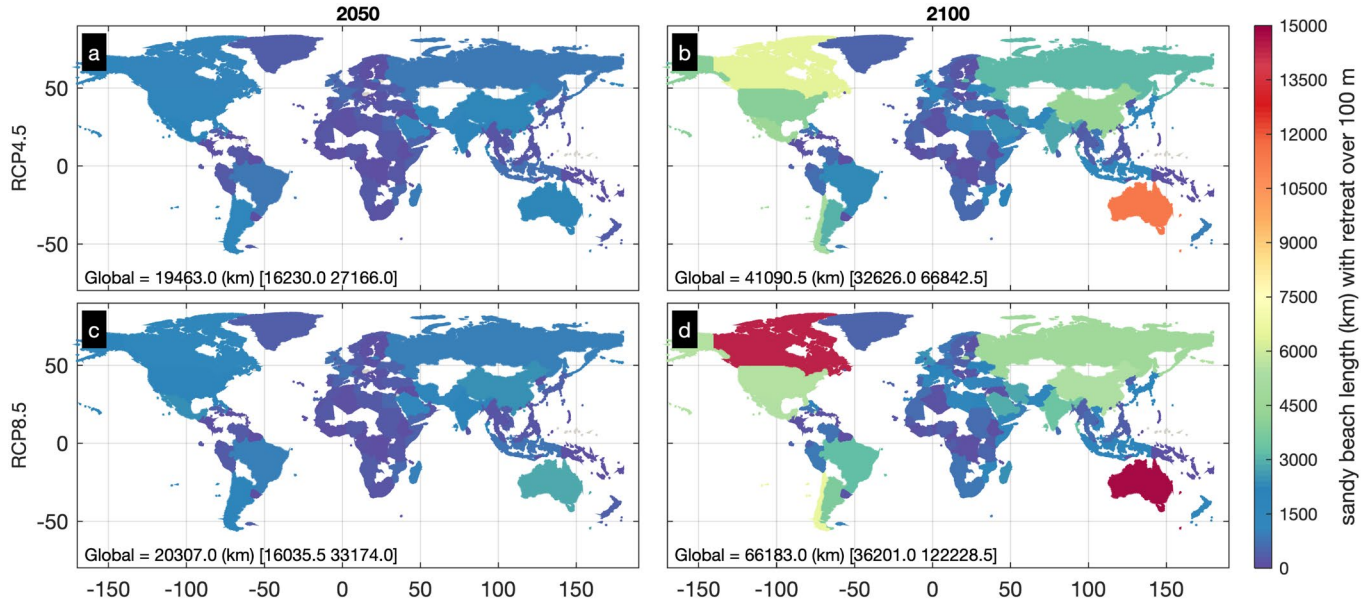

Extended Data Fig. 10 | Per country length of sandy beach shoreline that is projected to retreat by more than 100 m. Per country length of sandy beach coastline which is projected to retreat by more than 100 m by 2050 (a,c) and 2100 (b,d), under RCP4.5 (a-b) and RCP8.5 (c-d). Values are based on the median long-term shoreline change, relative to 2010.